Cross sections for elastic electron collisions with tetrahydrofuran

M. G. P. Homem,[1] R. T. Sugohara,[2] I. P. Sanches,[1] M. T. Lee,[1] and I. Iga[1]
[1]*Departamento de Química, UFSCar, 13565-905 São Carlos, SP, Brazil*
[2]*Departamento de Física, UFSCar, 13565-905 São Carlos, SP, Brazil*

(Received 18 May 2009; revised manuscript received 12 August 2009; published 8 September 2009)

In this work, we report an experimental cross-section determination of elastic electron collisions with tetrahydrofuran in the intermediate-energy range. More specifically, absolute differential cross sections are measured and reported in the (50–1000) eV range. The measurements were performed using a crossed electron beam–molecular beam geometry. The angular distributions of the scattered electrons were converted to absolute cross sections using the relative flow technique. A procedure based on the method of initial rate is applied to determine the flow rate of vaporized liquid samples. Moreover, integral and momentum transfer cross sections are derived from the measured differential cross sections. Comparison is made between our measured data with the existing experimental results and with our theoretical results calculated using the independent atom model at the static-exchange-polarization plus absorption level of approximation.

DOI: 10.1103/PhysRevA.80.032705 PACS number(s): 34.80.Bm

I. INTRODUCTION

Recent findings on the possibility that slow electrons may induce single- and double-strand breaks in DNA [1,2] have stimulated considerable interest, both experimental and theoretical, on electron interactions with subunits of DNA and RNA and with constituents of the backbone. It is well known that ionizing radiation is used widely in medicine as a probe in radiodiagnostic examinations and as a genotoxic agent in radiotherapy. When entering the body, high energy ionizing radiation quickly thermalizes through various scattering processes that liberate large numbers of low energy secondary electrons. These electrons then interact with biomolecules such as sugar [3] and DNA bases [4,5] and have been shown to cause significant damage to DNA through the process of dissociative attachment [1,6] leading either to direct single or double DNA strand breaks or to the formation of free radicals, which can then chemically react with DNA to lead to strand breaking. Therefore, cross-section data set for electron collisions with biomolecules would be of interest in estimating and modeling of processes induced by electrons within a molecular sample. In particular, the electron scattering cross sections, both differential and integral, are the input parameters for energy deposition modeling that is based on a Monte Carlo simulation of the single electron scattering process [7].

Nevertheless, relatively less attention has been given to electron interactions with constituents of the DNA backbone. Specifically for tetrahydrofuran (THF) which is a model for DNA backbone, to date, there are four experimental determinations of cross sections for elastic electron collisions with this target reported in the literature. Differential cross sections (DCS) for elastic scattering in the 20–300 eV energy range and in the 10°–110° angular range were recently measured by Milosavljević *et al.* [8]. More recently, DCS in the 6.5–50 eV energy range covering the angular range between 10° and 130° were reported by Colyer *et al.* [9] and by Dampc *et al.* [10] in the 6–20 eV and 20°–180° ranges. Vibrationally elastic and excitation DCS at 0.1–20 eV energy range and 10°–180° angular range were reported by Allan [11]. In the overlapping energy range between 20 and 50 eV, significant discrepancies were observed among the experimental determinations particularly at scattering angles between 20° and 80°. In addition, grand-total cross sections (TCS) for THF at incident energies of 0.1–21 eV were measured by Zecca *et al.* [12] and also by Możejko *et al.* [13] at incident energies up to 370 eV.

On the theoretical side, several recent calculations at the *ab initio* level for elastic e^--THF collisions have appeared in the literature. Integral cross sections (ICS), both elastic and electronically inelastic, have been calculated for THF by Bouchiha *et al.* [14] using the *R*-matrix method, at collision energies from 1–10 eV. Trevisan *et al.* [15] have reported calculations of DCS and momentum transfer cross sections (MTCS) for this target using the complex Kohn variational method. Elastic ICS for both THF and phosphoric acid, which constitutes the remainder of the DNA backbone, have been computed by Tonzani and Greene [16] using a variation of the *R*-matrix method. More recently, Winstead and McKoy [17] calculated DCS, ICS, and MTCS for elastic electron scattering from deoxyribose and related molecules, including THF, using the Schwinger multichannel method. The calculated DCS of Winstead and McKoy are in very good agreement with the experimental data of Colyer *et al.* [9], Dampc *et al.* [10], and Allan [11] for incident energies below 20 eV. Nevertheless, at higher energies, significant differences are seen between the calculated and experimental DCS particularly for scattering angles larger than 40°. Probably, these differences reflect the important influences of inelastic scattering channels (including excitation and ionization processes) on the elastic scattering channel, not included in their calculations.

Considering the discrepancies between the existing experimental cross sections and especially considering that the data reported by Milosavljević *et al.* [8] are the only experimental set available above 50 eV, further DCS measurements at such energies are clearly of interest. In this work, we present an experimental study for elastic electron scattering from THF in the intermediate-energy range. Absolute DCS determined using the relative flow technique (RFT) [18,19] in the 50–1000 eV range are reported. ICS and MTCS in this energy range are also derived from the experimental DCS measured in the 5°–130° angular range and extrapolated to forward and backward directions. In order to better compare

our data of ICS with the TCS measured by Możejko *et al.* [13], we also estimate the contribution of the total ionization cross sections (TICS) using the well-known binary-encounter-Bethe (BEB) method [20]. Since ionization dominates the inelastic scatterings, the sum of our experimental ICS and BEB TICS may provide a good estimation for TCS and its comparison with the experimental data of Możejko *et al.* is meaningful.

In Sec. II, we present with some detail our experimental setup and the procedures. Section III outlines the calculation methods. Finally, in Sec. IV, we compare our results with the theoretical and experimental data available in the literature.

II. EXPERIMENTAL

Details of our experimental setup and procedure have already been presented in our previous works [21] and will only be briefly described here. A crossed electron beam–molecular beam geometry is used to measure the relative angular distribution of the scattered electrons at a given incident electron energy. The scattered electrons are energy filtered by a retarding-field energy selector with a resolution of about 1.5 eV. With this resolution, it is sufficient to distinguish inelastically scattered electrons resulted from electronic excitation for the molecule under study since the lowest excitation threshold of THF is around 6 eV [22]. Nevertheless, it is unable to separate those from vibrational excitation (VE) processes. Therefore, our measured DCS are indeed vibrationally summed. The ratio between the VE and the vibrationally summed cross sections for THF was determined by Allan [11] at 6 and 10 eV. At 10 eV, the contribution of the VE processes is about 12% of the vibrationally summed cross sections. However, with increasing incident energies, the VE cross sections decrease much faster than the vibrational elastic cross sections. Therefore, we estimate that the VE contributions shall not exceed 3% at incident energies of 50 eV and above.

In our experiment, the gas beam is injected into the vacuum tank through a single molybdenum tube with inner diameter $d=1.0$ mm and length $L=30.0$ mm, aspect ratio $\gamma=d/L=0.033$. During the measurements, the working pressure in the vacuum chamber is between 0.2 to 2×10^{-6} torr. THF in gaseous phase is obtained from the saturated vapor above a liquid sample in a small vial attached to the gas handling system. The liquid sample of THF, with purity better than 99%, underwent a pretreatment in order to eliminate possible contaminants, mostly atmospheric air, through several freeze-thaw cycles. Liquid THF has relatively high vapor pressure at the room temperature, 165 torr at 25 °C [23]. When the pressure inside of the vial is reduced through pumping to levels below the saturation pressure, liquid THF suffers superheating. Therefore, the pressure inside of vacuum tank is unstable. In order to avoid this problem, during the measurements the liquid sample was maintained at the temperature of 0 °C in an ice and water bath. Using this procedure, a very stable molecular beam of THF can be generated. The purity of the gaseous sample is checked from time to time by a quadrupole mass spectrometer.

The recorded scattering intensities are converted into absolute elastic DCS (σ_D) using the RFT [18,19]. According to Eq. (6) of Nickel *et al.* [19], the intensity of the electrons scattered by a target per unity of incident electron beam current can be expressed as

$$I(E,\theta)=\frac{\eta\sigma_D(E,\theta)}{v}\beta, \tag{1}$$

where I is the scattered electron intensity, E is the impact energy, θ is the nominal scattering angle, η is the efficiency of the detection system, v is the mean velocity of molecules in the gaseous beam, and β is the result of the integral defined in Eq. (5) in Nickel *et al.* [19]. That integral is not trivial to be solved since its integrand depends on the scattering geometry as well as some beam properties such as spatial and velocity distributions, which are difficult to be determined experimentally. Nevertheless, the relative elastic intensities measured for the gas under study (x) and a secondary standard (std) are related to the corresponding cross sections as

$$\frac{I_x}{I_{std}}(E,\theta)=\left(\frac{M_x}{M_{std}}\right)^{1/2}\frac{\beta_x\sigma_{D,x}(E,\theta)}{\beta_{std}\sigma_{D,std}(E,\theta)}, \tag{2}$$

where M is the molecular weight. If the beam profiles of the two gases are closely the same, then it can be shown [19] that

$$\frac{\beta_{std}}{\beta_x}=\frac{n_{std}}{n_x}, \tag{3}$$

which is just the relative flow rate, n, for the two gases. Therefore, the DCS for a gas under determination can be related with known DCS of a secondary standard as

$$(\sigma_D)_x=(\sigma_D)_{std}\frac{I_x}{I_{std}}\frac{n_{std}}{n_x}\left(\frac{M_{std}}{M_x}\right)^{1/2}. \tag{4}$$

The validity of the above equation requires that the beam profiles of both gases x and std are closely the same. According to Olander and Kruger [24], this requirement is fulfilled under two conditions: the equal mean free paths (λ) of the gases in the gas reservoir behind the molybdenum tube and the Knudsen number K_L defined as $\frac{\lambda}{L}$ varying between $\gamma \leq K_L \leq 10$. However, several recent investigations have provided experimental evidences that even at beam flow regimes in which the K_L's are significantly lower than γ, the above relationship can still be valid [21]. In addition, Buckman *et al.* [25] investigated the spatial profiles of molecular beams for several gases. They found that the full width at half maximum of the beam profiles were very similar for Ar, Ne, N_2, and Kr in a wide range of λ (from 0.005 to 5 mm).

In the present study, Ar and N_2 are used as secondary standards. Absolute DCS for Ar in the 200–1000 eV energy range measured by Jansen *et al.* [26] and for N_2 in the 50–100 eV energy range of Dubois and Rudd [27] are used to normalize our data. In principle, the intensities of scattered electrons by THF and the secondary standards for a given angle should be measured using the ratio of pressures that ensures the equal mean-free-path condition, that is

$$P_{THF}:P_{std} = \delta_{std}^2:\delta_{THF}^2, \tag{5}$$

where δ is the molecular diameter. Using the diameters, δ_{Ar}=2.94 Å, δ_{N_2}=3.14 Å, and δ_{THF}=4.41 Å, calculated from the published van der Waals constants [23], the ratios are 0.44 and 0.51, respectively, for Ar and N_2 as secondary standards.

In this study, the initial-rate method is used to determine relative flow rates of both target and secondary standard gases. The mechanism of possible adsorption-desorption of gases on the surfaces is considered. This procedure is described as follows. During the scattering measurement, the pressure P_0 inside of the gas reservoir is constant. Moreover, there is also an equilibrium between the gas adsorption and desorption on the surfaces. Therefore, the inflow rate of the target gases via the leak valve is equal to the outflow rate through the molybdenum tube. To determine the flow rate under this condition, the method of pressure decrease is used. The inlet leak valve is shut off when the equilibrium is achieved and pressure versus time (P-t) is recorded. The variation in the pressure in the reservoir can be given approximately as

$$\frac{dP}{dt} = -k_1P - k_2P^2 + f_{des} - g_{ads}, \tag{6}$$

where the first two terms in the right-hand side of Eq. (6) are the effusion and the binary-collision processes, respectively, whereas f_{des} and g_{ads} correspond to the contributions of the gas desorption and adsorption on the surfaces. Higher-order P-dependent terms are neglected. At low pressures, the adsorption and desorption of gases can be well represented by Langmuir's model [28] as

$$g_{ads} = k_{ads}N(1-\Theta)P \tag{7}$$

and

$$f_{des} = k_{des}N\Theta. \tag{8}$$

In Eqs. (7) and (8), k_{ads} are k_{des} are rate constants for adsorption and desorption steps, respectively. N is the total number of gas-adsorption sites available on surfaces and Θ is the fraction of sites occupied by gaseous molecules. It is reasonable to assume that this fraction is proportional to the gas pressure inside of reservoir, that is $\Theta=\alpha P$, where α is a constant. Therefore, Eq. (6) can be rewritten as

$$\frac{dP}{dt} = -CP - DP^2, \tag{9}$$

where

$$C = k_1 - (k_{des}\alpha + k_{ads})N \tag{10}$$

and

$$D = k_2 - k_{ads}\alpha N. \tag{11}$$

The integration of Eq. (9) results in

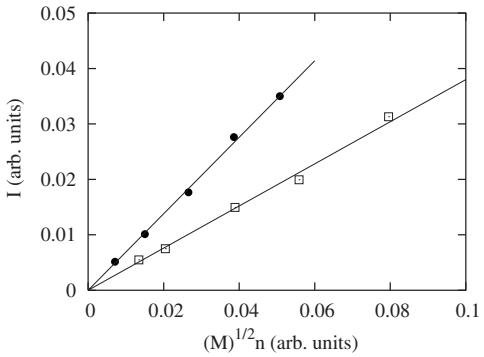

FIG. 1. Relative intensity of scattered electrons versus relative flow rate ($M^{1/2}n$) for Ar and THF at 1000 eV and 25° scattering angle. Solid circles, experimental data for THF; open squares, experimental data for Ar; full lines, the fittings of those data.

$$P = \frac{P_0e^{-Ct}}{1+\left(\frac{D}{C}\right)P_0 - \left(\frac{D}{C}\right)P_0e^{-Ct}}. \tag{12}$$

The values of C and D are obtained through a χ^2 fitting of this expression to the experimental P-t curve. In our study, the pressures at equilibrium, P_0, inside of reservoir are in the interval of 0.035–0.315 torr for THF and 0.08–0.4 torr for the standard gases. Very good fittings are obtained for these species. The outflow initial rate is given by $n=CP_0+DP_0^2$ for each gas.

Moreover, in our study, intensities of scattered electrons for THF and secondary standards at a given angle are recorded at several equilibrium pressures P_0. A typical plot of the scattering intensity I versus $M^{1/2}n$ is shown in Fig. 1 for THF and Ar at 1000 eV and 25°. It is seen that the measured values for both gases can be very well fitted to a linear function $y=bx$. Comparing to Eq. (1), the angular coefficient b can be written as

$$b = \left(\frac{\pi}{8kT}\right)^{1/2}\eta\frac{\beta}{n}\sigma_D(E,\theta), \tag{13}$$

where k is the Boltzmann constant and T is the temperature. This linear behavior of I is expected in molecular flow regime which seems not to be the case in this study. On the other hand, as pointed out by Nickel *et al.* [19], if the detector view cone covers the entire scattering region and the electron beam flux is uniform, the ratio $\frac{\beta}{n}$ becomes closely the same for all gases and so the relationship given in Eq. (3) is valid. Indeed, the view cone of our detector is quite large. In the scattering region, the diameter of the cone base is about 7 mm. Therefore, in our study the ratios of DCS are obtained directly via the ratio between the fitted angular coefficients. In addition, cross-checking tests were conducted using the equal mean-free-path condition and the obtained DCS have confirmed the validity of the procedure described above.

Details of the analysis of experimental uncertainties have also been given elsewhere [21]. They are estimated briefly as follows. Uncertainties of random nature such as pressure fluctuations, electron beam current readings, and background

scattering are estimated to be less than 2%. These contributions combined with the estimated statistical errors give an overall uncertainty of 4% in the relative DCS for each gas. Also, the experimental uncertainty associated with the normalization procedure is estimated to be 6%. These errors combined with the quoted errors of 6.5% in the absolute DCS of Ar of Jansen *et al.* [26] in the 200–1000 eV range provide an overall experimental uncertainty of 11% in our absolute DCS. At 50 eV and 100 eV, the quoted errors of the absolute DCS of N_2 of DuBois and Rudd [27] are 19% and 12%, respectively, which provide experimental uncertainties in our DCS of 21% at 50 eV and 15% at 100 eV. The absolute DCS were determined in the $5°-130°$ angular range. In order to obtain ICS and MTCS, an extrapolation procedure was adopted to estimate DCS at scattering angles out of the angular range covered experimentally. The extrapolation was carried out manually. The overall errors on ICS and MTCS are estimated to be 29% at 50 eV, 25% at 100 eV, and 23% elsewhere.

III. CALCULATION

In the IAM approach, the DCS for elastic electron scattering on a molecule, after averaging over the molecular orientations, is given as

$$\frac{d\sigma}{d\Omega} = \sum_{i}^{N} \sum_{j}^{N} f_i(\theta,k) f_j^*(\theta,k) \frac{\sin(sr_{ij})}{sr_{ij}}, \tag{14}$$

where N is the number of atoms within a molecule, r_{ij} is the internuclear distance, and $f_i(\theta,k)$ is the complex scattering amplitude due to the ith atom in a molecule. In Eq. (14), $s = 2k \sin(\frac{\theta}{2})$ is the magnitude of the transferred momentum during the collision and k is the magnitude of the linear momentum of the incident electron.

Moreover, atomic scattering amplitudes are obtained by solving the partial-wave radial Schrödinger equation

$$\left(\frac{d^2}{dr^2} - \frac{l(l+1)}{r^2} - 2V_{opt} + k^2\right) u_l(r) = 0, \tag{15}$$

where V_{opt} is the optical potential composed of the static, the exchange, the correlation-polarization and the absorption contributions. In the present work, the static atomic potentials used are those given by Salvat *et al.* [29]. A model potential proposed by Furness and McCarthy [30] is used to account for the exchange contributions. Moreover, a parameter-free model potential introduced by Padial and Norcross [31] is used to account for the correlation-polarization contributions. In this model, a short-range correlation potential between the scattering and the target electrons is defined in an inner interaction region and a long-range polarization potential in an outer region. The correlation potential is calculated by a free-electron-gas model derived using the target electronic density according to Eq. (9) of Padial and Norcross [31]. In addition, an asymptotic form of the polarization potential is used for the long-range electron-target interaction. The atomic polarizabilities as well as the internuclear distances used in the calculation are taken from the literature [23]. Finally, the absorption contributions were accounted for via the version 3 of the quasi-free scattering model potential of Staszewska *et al.* [32]. For the generation of exchange, polarization, and absorption contributions, atomic density functions are needed. They are also taken from the article of Salvat *et al.* [29].

The ICS $[\sigma_I(E)]$ and the MTCS $[\sigma_M(E)]$ for elastic electron-molecule scattering are defined as

$$\sigma_I(E) = 2\pi \int_0^{\pi} \frac{d\sigma}{d\Omega} \sin\,\theta d\theta \tag{16}$$

and

$$\sigma_M(E) = 2\pi \int_0^{\pi} \frac{d\sigma}{d\Omega} (1 - \cos\,\theta) \sin\,\theta d\theta, \tag{17}$$

respectively. Nevertheless, it should be pointed out that ICS calculated using Eq. (16) overestimate in general the experimental values by a factor of 2–3. In some recent studies [33], the optical theorem was applied to generate the ICS within the IAM formalism. However, it can be shown that such approach is in fact equivalent to the well-known additivity rule (AR). In the present study, both IAM and AR are used to estimate the ICS whereas MTCS are calculated using only IAM according to Eq. (17).

For a particular molecular orbital n, electron-impact partial ionization cross sections can be obtained using the BEB model [20] as

$$\sigma_n = \frac{S}{t+u+1}\left[\frac{\ln t}{2}\left(1 - \frac{1}{t^2}\right) + 1 - \frac{1}{t} - \frac{\ln t}{t+1}\right], \tag{18}$$

where $u = U/B$, $t = E/B$, and $S = 4\pi a_0^2 N R^2/B^2$, with N as the orbital occupation number and R as the Rydberg constant in electron volts. The orbital electron binding energy B and the kinetic energy U for the ground state are calculated within the Hartree-Fock framework using a 6–311G basis set. The PC GAMESS/FIREFLY QC package [34], which is partially based on the GAMESS (U.S.) source code [35] is used for these calculations. The TICS are obtained as a sum of the partial ionization cross sections of all molecular orbitals.

IV. RESULTS AND DISCUSSION

The present experimental data of DCS, ICS, and MTCS, for elastic e^--THF collisions, obtained in the 50–1000 eV energy range, are presented in Table I. In Figs. 2–4 we present our absolute DCS for electron scattering by THF in the 50–1000 eV incident energy range along with our calculated DCS using the IAM.

The experimental DCS of Milosavljević *et al.* [8] in the 50–300 eV energy range are also shown for comparison. Specifically at 50 eV, we have also plotted the experimental data of Colyer *et al.* [9] and the theoretical DCS of Winstead and McKoy [17]. At that energy, our experimental DCS agree quite well, both qualitatively and quantitatively, with the measured data of Colyer *et al.* On the other hand, there is a significant disagreement, both in shape and magnitude, between our data and those of Milosavljević *et al.* at scattering

TABLE I. Experimental DCS, ICS, and MTCS (in 10^{-16} cm^2) for e^--THF scattering.

Angle (deg)	E_0 (eV)						
	50	100	200	300	400	500	1000
5			5.50(1)[a]	3.74(1)	2.95(1)	2.71(1)	1.45(1)
10	5.72(1)	3.05(1)	1.07(1)	1.31(1)	8.19(0)	5.37(0)	4.63(0)
15	2.23(1)	7.03(0)	5.41(0)	2.83(0)	3.39(0)	3.54(0)	2.25(0)
20	6.47(0)	3.25(0)	2.47(0)	2.40(0)	2.19(0)	1.91(0)	1.30(0)
25	2.85(0)	2.46(0)	1.81(0)	1.49(0)	1.20(0)	1.16(0)	4.82(−1)
30	1.82(0)	1.80(0)	1.15(0)	8.97(−1)	8.52(−1)	8.42(−1)	3.15(−1)
35	1.66(0)	1.25(0)					
40	1.12(0)	9.01(−1)	5.80(−1)	5.21(−1)	2.80(−1)	2.34(−1)	1.16(−1)
45	8.96(−1)	6.67(−1)					
50	8.00(−1)	5.18(−1)	3.05(−1)	1.59(−1)	1.78(−1)	1.69(−1)	6.14(−2)
55	5.57(−1)	4.69(−1)					
60	3.83(−1)	3.86(−1)	1.22(−1)	1.41(−1)	1.09(−1)	8.94(−2)	3.50(−2)
65	3.46(−1)	2.61(−1)					
70	2.85(−1)	2.11(−1)	1.17(−1)	9.95(−2)	6.71(−2)	6.45(−2)	2.08(−2)
75	2.61(−1)	1.82(−1)					
80	2.06(−1)	1.59(−1)	9.60(−2)	6.63(−2)	5.65(−2)	3.84(−2)	1.32(−2)
85	1.96(−1)	1.45(−1)					
90	2.08(−1)	1.56(−1)	8.37(−2)	5.30(−2)	4.40(−2)	3.51(−2)	1.02(−2)
95		1.82(−1)					
100	2.25(−1)	2.08(−1)	7.07(−2)	5.09(−2)	3.77(−2)	2.67(−2)	8.71(−3)
105	2.59(−1)	2.26(−1)					
110	3.11(−1)	2.42(−1)	6.51(−2)	5.03(−2)	3.65(−2)	2.06(−2)	6.53(−3)
115	3.36(−1)	2.66(−1)					
120	3.83(−1)	2.85(−1)	7.95(−2)	4.32(−2)	3.18(−2)	1.68(−2)	5.00(−3)
125		3.08(−1)					
130			8.20(−2)	4.71(−2)	2.96(−2)	1.96(−2)	4.67(−3)
ICS	2.43(1)	1.78(1)	8.97(0)	6.42(0)	5.46(0)	5.35(0)	2.88(0)
MTCS	6.43(0)	5.25(0)	1.62(0)	9.60(−1)	7.04(−1)	5.46(−1)	2.02(−1)

[a]5.50(1) means 5.50×10^{1}.

angles smaller than 90°. The calculated results of Winstead and McKoy are in fairly good agreement with our experimental data for angles up to 30°. At larger angles, their calculated results agree qualitatively with our data. However, the theory significantly overestimates the DCS, probably due to the neglect of absorption effects in their calculation.

It has already been pointed out [36,37] that the absorption effects can influence substantially the DCS for elastic electron-molecule scattering in the energies above 30 eV. Moreover, our calculated DCS using the IAM show qualitative agreement with our experimental data, although significantly overestimate the magnitude of DCS.

At 100 and 200 eV, there is an overall good agreement between the present experimental DCS and those of Milosavljević *et al.* The DCS calculated using the IAM are in qualitative agreement with our measured data. At 100 eV, reasonable quantitative agreement is also seen at scattering angles above 30°. However, at both energies, IAM calculation significantly overestimates the DCS at small angles.

At 300 eV, the DCS of Milosavljević *et al.* lie systematically below our measured data in the overlapping angular range. Also, the shape of their DCS does not show oscillations, in contrast to those seen in our data. Such oscillatory structures in DCS are probably due to the diffraction of electrons by nuclei. Again, IAM DCS agree qualitatively with our measured data, but significantly overestimate the magnitude at small scattering angles.

At 500 and 1000 eV, there is no existing experimental or theoretical data of DCS in the literature, therefore, comparison is made only with our calculated results using the IAM. At such high incident energies, very good agreement, both in shape and magnitude, between the theory and experiment is seen, except at the scattering angles near forward direction where the IAM DCS are still too large. The systematic DCS overestimation by IAM at small scattering angles is possibly due to the manner that the contribution of the polarization effects is accounted for. In IAM calculations, the polarization potential is calculated separately for each atom. Neverthe-

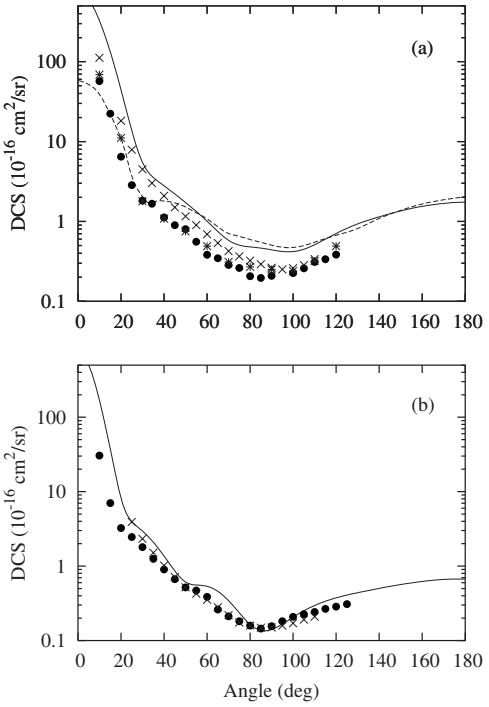

FIG. 2. DCS for elastic e^--THF scattering at (a) 50 eV and (b) 100 eV. Full line, present calculated data using the IAM; dashed line, theoretical results of Winstead and McKoy [17]; full circles, present experimental data; crosses, experimental DCS of Milosavljević *et al.* [8]; asterisk, experimental DCS of Colyer *et al.* [9].

less, the sum of the polarizabilities of the constituent atoms is much larger than the molecular polarizability. This behavior has already been observed in our previous work for hydrocarbon molecules [38].

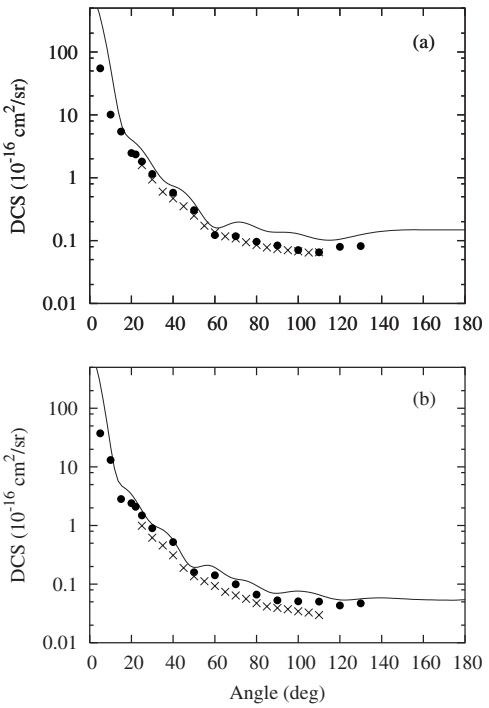

FIG. 3. The same as in Fig. 2, but for (a) 200 eV and (b) 300 eV.

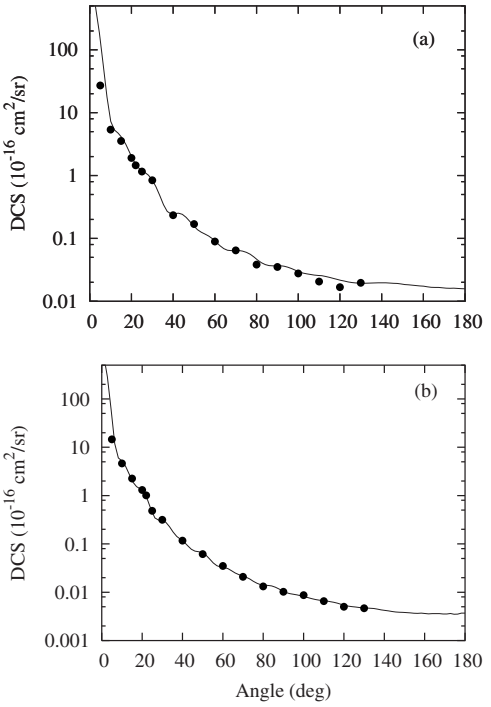

FIG. 4. The same as in Fig. 2, but for (a) 500 eV and (b) 1000 eV.

In Figs. 5(a) and 5(b) we present, respectively, our experimental ICS and MTCS for elastic electron scattering by THF in the 50–1000 eV energy range along with the experimental

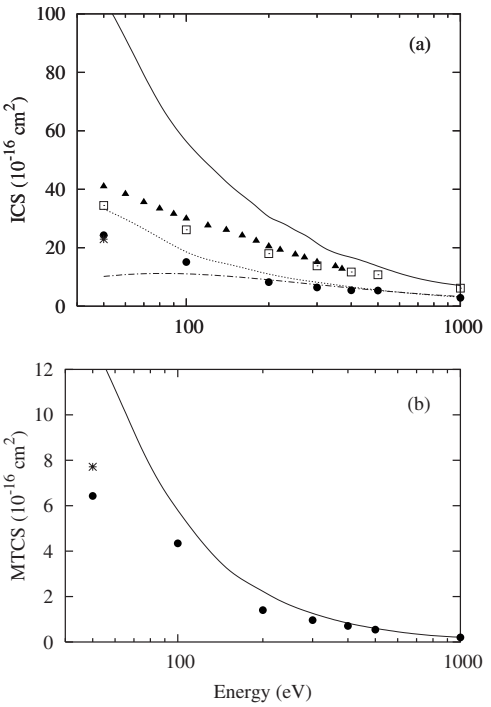

FIG. 5. (a) ICS and (b) MTCS for elastic e^--THF scattering in the 50–1000 eV range. Full curve, present IAM results; dashed line, present calculated results using the additivity rule; full circles, present experimental data; asterisk, experimental results of Colyer *et al.* [9]; dashed-dotted line, present TICS calculated using BEB; open squares, sum of present experimental ICS and theoretical TICS; full triangles, experimental TCS of Możejko *et al.* [13].

data of Colyer *et al.* at 50 eV, in comparison with the corresponding calculated data using the AR and IAM. The TCS measured by Możejko *et al.*, present calculated TICS using the BEB model as well as the sum of our ICS and TICS are also shown for comparison. At 50 eV, our experimental ICS and MTCS are in good agreement with those reported by Colyer *et al.* It is also seen that the ICS calculated by IAM lie well above our experimental data in the entire energy range covered herein whereas the agreement between AR ICS and our experimental data is fairly good except at 50 eV. In addition, there is also a good agreement between the MTCS computed using the IAM and the experimental data for energies of 100 eV and above. The TCS of Możejko *et al.* lie systematically above our ICS which is physically consistent, since TCS also account for contributions from inelastic processes. It is interesting to note that the sum of our TICS and ICS agrees quite well with experimental TCS of Możejko *et al.* for incident energies of 300 eV and above. At lower energies, this sum lies slightly below the experimental TCS which can probably be attributed to the neglect of contributions from electronic excitation processes.

In summary, in this work we report an experimental investigation on elastic electron scattering by THF in the 50–1000 eV energy range. At 50 eV, our data are in good agreement with those reported of Colyer *et al.* but deviate significantly from those of Milosavljević *et al.* both in shape and magnitude. The agreement between our DCS and those of Milosavljević *et al.* improves at 100 and 200 eV, but significant deviations are again seen at 300 eV. Moreover, in general the DCS calculated using the IAM agree qualitatively with our experimental data at the incident energies covered herein. At 500 eV and above, very good quantitative agreement is also verified.

ACKNOWLEDGMENTS

This research was partially supported by the Brazilian agencies FAPESP, CNPq, and CAPES.

[1] B. Boudaïffa, P. Cloutier, D. Hunting, M. A. Huels, and L. Sanche, Science **287**, 1658 (2000).
[2] M. A. Huels, B. Boudaïffa, P. Cloutier, D. Hunting, and L. Sanche, J. Am. Chem. Soc. **125**, 4467 (2003).
[3] S. Ptasińska, S. Denifl, P. Scheier, and T. D. Märk, J. Chem. Phys. **120**, 8505 (2004).
[4] H. Abdoul-Carime, S. Gohlke, and E. Illenberger, Phys. Rev. Lett. **92**, 168103 (2004).
[5] K. Aflatooni, A. M. Scheer, and P. D. Burrow, J. Chem. Phys. **125**, 054301 (2006).
[6] F. Martin, P. D. Burrow, Z. Cai, P. Cloutier, D. Hunting, and L. Sanche, Phys. Rev. Lett. **93**, 068101 (2004).
[7] H. Nikjoo, S. Uehara, D. Emfietzoglou, and F. A. Cucinotta, Radiat. Meas. **41**, 1052 (2006).
[8] A. R. Milosavljević, A. Giuliani, D. Sević, M. J. Hubin-Franskin, and B. P. Marinković, Eur. Phys. J. D **35**, 411 (2005).
[9] C. J. Colyer, V. Vizcaino, J. P. Sullivan, M. J. Brunger, and S. J. Buckman, New J. Phys. **9**, 41 (2007).
[10] M. Dampc, A. R. Milosavljević, I. Linert, B. P. Marinković, and M. Zubek, Phys. Rev. A **75**, 042710 (2007).
[11] M. Allan, J. Phys. B **40**, 3531 (2007).
[12] A. Zecca, C. Perazzolli, and M. J. Brunger, J. Phys. B **38**, 2079 (2005).
[13] P. Możejko, E. Ptasińska-Denga, A. Domaracka, and C. Szmytkowski, Phys. Rev. A **74**, 012708 (2006).
[14] D. Bouchiha, J. D. Gorfinkiel, L. G. Caron, and L. Sanche, J. Phys. B **39**, 975 (2006).
[15] C. S. Trevisan, A. E. Orel, and T. N. Rescigno, J. Phys. B **39**, L255 (2006).
[16] S. Tonzani and C. Greene, J. Chem. Phys. **125**, 094504 (2006).
[17] C. Winstead and V. McKoy, J. Chem. Phys. **125**, 074302 (2006).
[18] S. K. Srivastava, A. Chutjian, and S. Trajmar, J. Chem. Phys. **63**, 2659 (1975).
[19] J. C. Nickel, P. W. Zetner, G. Shen, and S. Trajmar, J. Phys. E **22**, 730 (1989).
[20] Y.-K. Kim and M. E. Rudd, Phys. Rev. A **50**, 3954 (1994).
[21] P. Rawat, I. Iga, M. T. Lee, L. M. Brescansin, M. G. P. Homem, and L. E. Machado, Phys. Rev. A **68**, 052711 (2003).
[22] A. Giuliani, P. Limão-Vieira, D. Duflot, A. R. Milosavljević, B. P. Marinković, S. V. Hoffmann, N. Mason, J. Delwiche, and M.-J. Hubin-Franskin, Eur. Phys. J. D **51**, 97 (2009).
[23] *Handbook of Chemistry and Physics*, 73rd ed., edited by David R. Lide (CRC Press, Boca Raton, 1992).
[24] D. R. Olander and V. Kruger, J. Appl. Phys. **41**, 2769 (1970).
[25] S. J. Buckman, R. J. Gulley, M. Moghbelalhossein, and S. J. Bennett, Meas. Sci. Technol. **4**, 1143 (1993).
[26] R. H. J. Jansen, F. J. de Heer, H. J. Luyken, B. van Wingerden, and H. J. Blaauw, J. Phys. B **9**, 185 (1976).
[27] R. D. DuBois and M. E. Rudd, J. Phys. B **9**, 2657 (1976).
[28] P. W. Atkins, *Physical Chemistry*, 5th ed. (Oxford University Press, Oxford, 1994).
[29] F. Salvat, J. D. Martinez, R. Mayol, and J. Parellada, Phys. Rev. A **36**, 467 (1987).
[30] J. B. Furness and I. E. McCarthy, J. Phys. B **6**, 2280 (1973).
[31] N. T. Padial and D. W. Norcross, Phys. Rev. A **29**, 1742 (1984).
[32] G. Staszewska, D. W. Schwenke, D. Thirumalai, and D. G. Truhlar, Phys. Rev. A **28**, 2740 (1983).
[33] P. Możejko and L. Sanche, Radiat. Phys. Chem. **73**, 77 (2005).
[34] A. A. Granovsky, PC GAMESS/FIREFLY version 7.1.F, http://classic.chem.msu.su/gran/gamess/index.html
[35] M. W. Schmidt, K. K. Baldridge, J. A. Boatz, S. T. Elbert, M. S. Gordon, J. H. Jensen, S. Koseki, N. Matsunaga, K. A. Nguyen, S. Su, T. L. Windus, M. Dupuis, and J. A. Montgomery, J. Comput. Chem. **14**, 1347 (1993).
[36] M.-T. Lee, I. Iga, L. E. Machado, L. M. Brescansin, E. A. y Castro, I. P. Sanches, and G. L. C. de Souza, J. Electron Spectrosc. Relat. Phenom. **155**, 14 (2007).
[37] E. A. y Castro, G. L. C. de Souza, I. Iga, L. E. Machado, L. M. Brescansin, and M.-T. Lee, J. Electron Spectrosc. Relat. Phenom. **159**, 30 (2007).
[38] I. P. Sanches, R. T. Sugohara, L. Rosani, M.-T. Lee, and I. Iga, J. Phys. B **41**, 185202 (2008).